Arginine/2,5-Dihydroxybenzoic Acid Clusters: An Experimental and Computational Study of the Gas-Phase and Solid-State Systems†

Gary R. Kinsel,‡ Qingchun Zhao,‡ Jayakumar Narayanasamy,‡ Faten Yassin,‡ H. V. Rasika Dias,‡ Bradley Niesner,‡ Katherine Prater,§ Chris St. Marie,§ Le Ly,§ and Dennis S. Marynick*,‡

Department of Chemistry and Biochemistry, University of Texas at Arlington, Arlington, Texas 76019-0065, and Chemistry Department, Texas Wesleyan University, Ft. Worth, Texas 76105-1536

Received: October 30, 2003; In Final Form: January 12, 2004

The 1:1 adduct of arginine with 2,5-dihydroxybenzoic acid (DHB) has been studied in the gas phase and in the solid state. Experimentally, the ionization energy (IE) of the 1:1 cluster was determined by wavelength-dependent laser ionization of clusters formed by seeding DHB and arginine into a supersonic jet expansion. Ionization laser power studies performed at several discrete wavelengths established the upper and lower limits for the 1:1 cluster IE and dissociation energy. Subsequent one-color scanned-wavelength laser ionization studies allowed an experimental establishment of the 1:1 cluster IE of 7.193 eV. A combination of molecular dynamics/simulated annealing calculations on the 1:1 cluster followed by density functional theory geometry optimizations using reasonably large basis sets yielded 15 distinct minima on the potential energy surface, all within 5.2 kcal/mol in energy at the B3LYP/6-311++G(2df,2p)//B3LYP/6-31+G** level. The Boltzmann-averaged IE at the same level is 7.11−7.14 eV, in excellent agreement with experiment. Cocrystals of arginine and DHB have been grown, and the crystal structure has been solved. The dominant intermolecular interaction in the cocrystal is a double hydrogen bond (salt bridge) between the guanidinium group of arginine and the (deprotonated) carboxylate group of DHB. This is exactly the same interaction that is found in the lowest-energy structure of the gas-phase 1:1 adduct. The electronic structure of the solid-state cocrystal has been modeled using a cluster approach.

Introduction

Hydrogen-bonding interactions play a central role in biochemistry. Of particular interest are hydrogen bonds involving amino acids. Over the years, considerable attention has been paid to the existence (or more properly the nonexistence) of the zwitterionic forms of the amino acids in the gas phase.[1−6] While all amino acids can exist as zwitterions in solution, the stability of the zwitterionic form is thought to be associated with solvation effects (essentially hydrogen bonding), which stabilize the NH_3^+ and COO^- groups of the zwitterion.

Recently arginine, the most basic of all the amino acids, has been the focus of a great deal of work. The impetus for much of this work was a suggestion[7] in 1997 that arginine exists as a zwitterion in the gas phase. However, subsequent experimental work[8] using infrared cavity ringdown laser absorption spectroscopy and high-level theoretical calculations[6,9] point to arginine existing in the canonical form in the gas phase, although the energy differences are not large. Indeed, high-level theoretical work on the arginine dimer and trimer demonstrates that these species *are* zwitterionic in the gas phase, with the dominant bonding interaction being the guanidinium/carboxylate salt bridges.[10]

Our own interest in this subject arises from an ongoing research program dealing with fundamental issues surrounding the mechanism of matrix-assisted laser desorption/ionization (MALDI) mass spectrometry.[11] In MALDI, an analyte (typically a protein) is codeposited with a matrix (typically a small organic molecule with an aromatic moiety) and subsequently desorbed into the gas phase. Because the matrix is likely a proton donor, the details of the molecular interactions between the matrix and the analyte are important for the understanding of the MALDI process. Our approach has been to study a number of model systems using a variety of experimental and computational techniques.[12−15]

In this paper, we study the interaction of a common MALDI matrix, 2,5-dihydroxybenzoic acid (DHB) with arginine. We show that the gas phase 1:1 cluster has an ionization energy (IE) of 7.193 eV, well below that of pure DHB (8.05 eV).[16] Molecular dynamics/simulated annealing calculations followed by geometry optimizations at the density functional theory (DFT) level reveal that most of the minima on the arginine−DHB potential energy surface share a unique feature; the arginine is protonated by the DHB to form an ion-pair cluster, while the arginine itself remains in the canonical (not zwitterionic) form. The calculated IE is 7.11−7.14 eV, in near perfect agreement with experiment. In addition, we have cocrystallized the 1:1 adduct of arginine and DHB. X-ray crystallographic analysis reveals a similar bonding pattern, with the DHB deprotonated and the arginine in the protonated zwitterionic form. Finally, the electronic structure of the solid-state cocrystal is modeled using a cluster approach.

Experimental Section

Laser Ionization Mass Spectrometry. All laser ionization mass spectrometry experiments are performed on a laboratory-

† Part of the special issue "Fritz Schaefer Festschrift".

* Author to whom correspondence may be addressed. E-mail: dennis@uta.edu.

‡ University of Texas at Arlington.

§ Texas Wesleyan University.

10.1021/jp031207s CCC: $27.50 © 2004 American Chemical Society
Published on Web 02/17/2004

constructed laser desorption/supersonic jet entrainment/linear time-of-flight mass spectrometer (TOFMS). Samples are prepared by first dissolving DHB and arginine (R) in excess methanol and then allowing the solvent to evaporate to form a crystalline mixture of the two components. The crystalline mixture is then ground to a fine powder, and the powder is pressed into a slotted sample holder to form a layer approximately 1 mm thick. The sample holder is then mounted on a motorized translation stage that, when inserted into the laser desorption region, translates the sample approximately 2 mm below the 800-μm opening of a high-pressure pulse valve (General Valve, Fairfield, NJ).

Laser desorption of the crystalline sample is performed using the softly focused, frequency-quadrupled output of a Nd−YAG laser (Continuum Minilite, Santa Clara, CA) at 266 nm. Following laser desorption, the high-pressure pulse value is opened to emit a 10-μs pulse of argon (backing pressure 190 psia) perpendicular to the normal of the sample surface. The laser-desorbed material is entrained in the argon pulse and transported ca. 1.5 cm where the majority of the material is transmitted through a skimmer having a 3-mm diameter opening into the TOFMS.

The neutral laser-desorbed material enters the ion-source region of the TOFMS axially through a 4-mm hole in the center of the repeller electrode. Any ionized material is prevented from entering the ion source region as a result of the continuous high-voltage bias applied to the repeller electrode. Laser ionization of the neutral material is performed using one of several lasers; 308-nm radiation is provided by an XeCl excimer laser (Lambda Physik LPX200, Ft. Lauderdale, FL); 355- and 266-nm radiation are provided by the frequency-tripled and -quadrupled outputs of a Nd−YAG laser (Continuum Surelite-II, Santa Clara, CA), and tunable radiation is provided by the frequency-doubled output of a dye laser (Lambda Physik FL3002, Ft. Lauderdale, FL) pumped by the Nd−YAG laser.

The output of the selected laser source is constrained by a 4-mm diaphragm before passing through the center of the ion-source region of the TOFMS. Adjustment of the intensity of the laser source to achieve ion formation is achieved through the use of attenuation plates and/or changes in the laser pump voltage. In cases where higher laser powers are required, a cylindrical lens ($f = 14.5$ mm at 266 nm) is used to focus the laser source into the center of the ion-source region. All ions produced as a result of laser excitation are accelerated using continuous bias voltages of 5.3, 4.7, and 0 kV applied to the repeller, 1st, and 2nd acceleration electrodes, respectively. Accelerated ions separate in time and space as they travel a distance of 1 m prior to striking a microsphere detector (El-Mul, Israel) attached to digital storage oscilloscope (LeCroy 9350, Chestnut Ridge, NY). Synchronization of the opening of the pulse valve and the firing of the desorption and ionization lasers is performed using a digital delay generator (Stanford Research Instruments DG535, Sunnyvale, CA) operated at a repetition rate of 5 Hz.

For the photoionization efficiency studies the frequency-doubled output of two laser dyes, DCM and LDS698, are used to cover the wavelength range from 308 to 355 nm. In these experiments, mass spectra are acquired at a series of wavelengths using the highest ionization laser power that yields only $DHB_1R_1^{+\bullet}$ in the mass spectrum. Appearance of fragments of $DHB_1R_1^{+\bullet}$, and especially appearance of RH^+, is taken as an indication of the onset of three-photon processes (see results section). Six mass spectra are acquired at each wavelength, and the average integrated area of the $DHB_1R_1^{+\bullet}$ ion signal is used for plotting the photoionization efficiency curve.

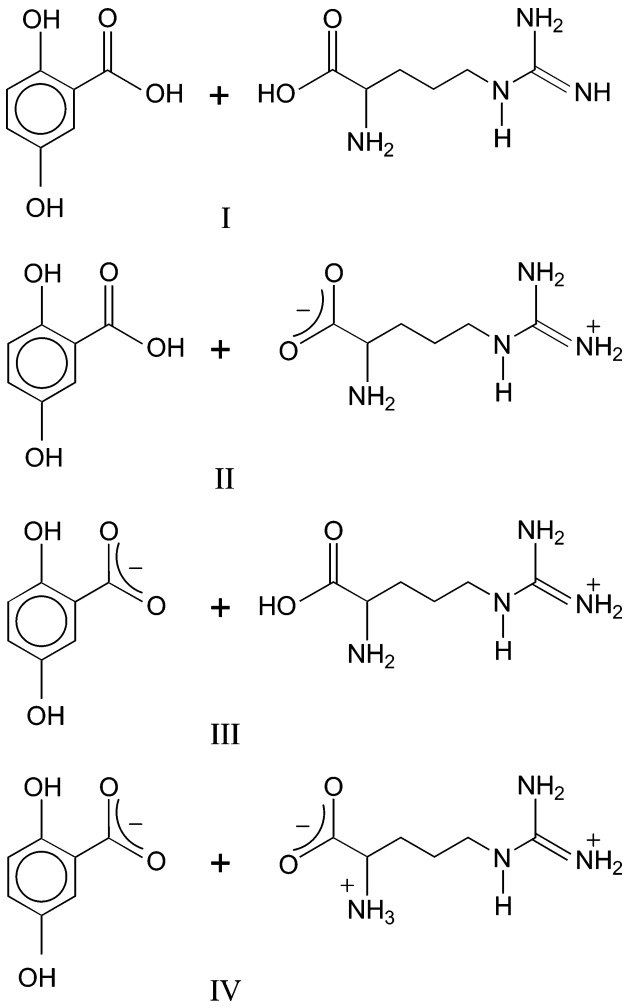

Figure 1. Starting points for molecular dynamics simulations. (I) DHB + canonical arginine, (II) DHB + zwitterionic arginine, (III) deprotonated DHB + canonical protonated arginine, and (IV) deprotonated DHB + zwitterionic protonated arginine.

Crystal Growth. Cocrystals of DHB and arginine were grown by dissolving equimolar mixtures of DHB and arginine in a 50:50 (v/v) water/acetonitrile solvent with sonication. A small string was suspended in the solution to aid crystal nucleation, and the sample vial containing the solution was subsequently loosely covered and placed in a refrigerator maintained at 5 °C. Formation of the DHB−arginine cocrystals was observed to occur in the solution after approximately 2 days, after which time the sample vial was tightly capped to prevent further evaporation of the solvents prior to X-ray crystallographic analysis.

X-ray Structure Determination. A suitable crystal covered with a layer of hydrocarbon oil was selected and attached to a glass fiber using epoxy glue. Data collections were carried out at room temperature on a Siemens P4 diffractometer equipped with a graphite monochromated Mo Kα radiation ($\lambda = 0.710$ 73 Å) source. The unit-cell parameters were determined by least-squares refinement of 39 reflections. Three standard reflections were measured at every 97 data points to check for crystal deterioration and/or misalignment. No significant deterioration in intensity was observed. Data were corrected for Lorentz, polarization, and absorption (using ψ scans) effects. Structures were solved by direct methods followed by successive cycles of full-matrix least-squares refinement on F^2 and difference

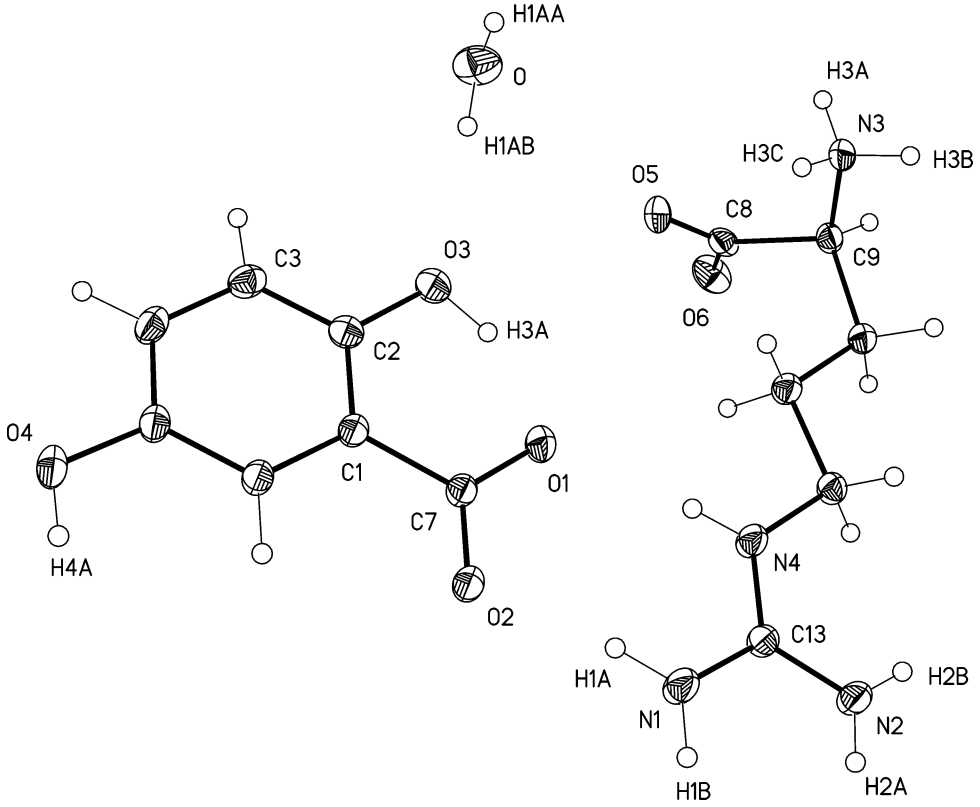

Figure 2. Asymmetric unit of the arginine−DHB cocrystal.

Fourier analysis. Arginine and DHB form 1:1 adducts and crystallize with a molecule of water in the crystal lattice. All hydrogen atoms were located from the difference map and refined with isotropic displacement parameters. All the non-hydrogen atoms were refined anisotropically. Software programs and the sources of scattering factors are contained in the Bruker SHELXTL 5.1 software package provided by the Bruker Analytical X-ray Instruments, Inc.

Computational

Gas-Phase Modeling. Molecular dynamics and simulated annealing were performed to identify the candidate structures starting from (I) DHB + canonical arginine, (II) DHB + zwitterionic arginine, (III) deprotonated DHB + canonical-protonated arginine, and (IV) deprotonated DHB + zwitterionic-protonated arginine (Figure 1). In system IV, we considered the arginine as a zwitterionic structure with the α- amino group protonated, as seen in the crystal structure (see below). Several different force fields, including MM2,[17] Amber,[18] and MMFF[19] were used to find the candidate structures. In general, MMFF yielded the most satisfactory structures. During the molecular dynamics (MD) simulations, the systems were heated to 1300 K in 35 ps followed by a run time of 40 ps and cooled to 20 K in 35 ps. The candidate structures were then optimized at the HF/6-31G* level. All structures within 10 kcal/mol of the lowest-energy structure at this level were then optimized at the B3LYP/6-31+G** level[20,21] of theory, and vibrational frequencies were obtained to verify that each structure is a minimum on the potential energy surface. Final energetics were calculated at the B3LYP/6-311++G(2df,2p)//B3LYP/6-31+G** level.[22] Vertical IEs were calculated as the energy difference between the neutral and ionized species at the geometry of the neutral species. Because there are several energetically competitively structures, the IEs were Boltzmann averaged using the free energies obtained at the B3LYP/6-31+G** level except for the base electronic energies, which were taken from the B3LYP/6-311++G(2df,2p) level. As a final check of the relative energies of the various conformers, single-point calculations at the MP2/6-31+G(2df,2p)//B3LYP/6-31+G** level were performed.[23]

The MD simulations were carried out using macromodel 8.1[24] from Schrodinger, Inc. Ab initio and DFT calculations were carried out using the Gaussian 98 suite of programs.[25]

Solid-State Modeling. We developed a simple model to probe the effects of the cocrystal on the electronic structure of DHB. We identified the strongly interacting part of the system, which is treated explicitly. This consists of one arginine, one DHB, and one water molecule (Figure 2). We call this the "fundamental unit" of the cocrystal. The arginine and DHB are double hydrogen bonded through the DHB carboxylate group and the arginine guanidinium group. The water molecule is hydrogen bonded to the DHB molecule at the 2-OH group. Substituting electrostatic potential derived atomic point charges on an atom-by-atom basis accounts for the remaining part of the crystal. These calculations employed both Hartree−Fock and density functional methods with the 6-31+G** basis set. Since X-ray diffraction yields systematically short bonds to hydrogen, all OH, NH, and CH bonds were adjusted to 1.029, 1.038, and 1.079 Å, respectively.[26] Changes in the IE can obviously be due to a ground-state effect or an ion-state effect. To differentiate between these effects, Koopmans' theorem[27] IEs (KTIEs) were also calculated at the HF/6-31+G** level. The KTIE of a molecule is essentially the negative of the energy of the highest occupied molecular orbital of the un-ionized species and therefore measures ground-state but not ion-state effects.

This cocrystal is monoclinic with the *P*2(1) space group. Applying the symmetry operations of the space group generated the full unit cell. Then, to generate large cocrystals, the coordinates of the first unit cell were translated with different

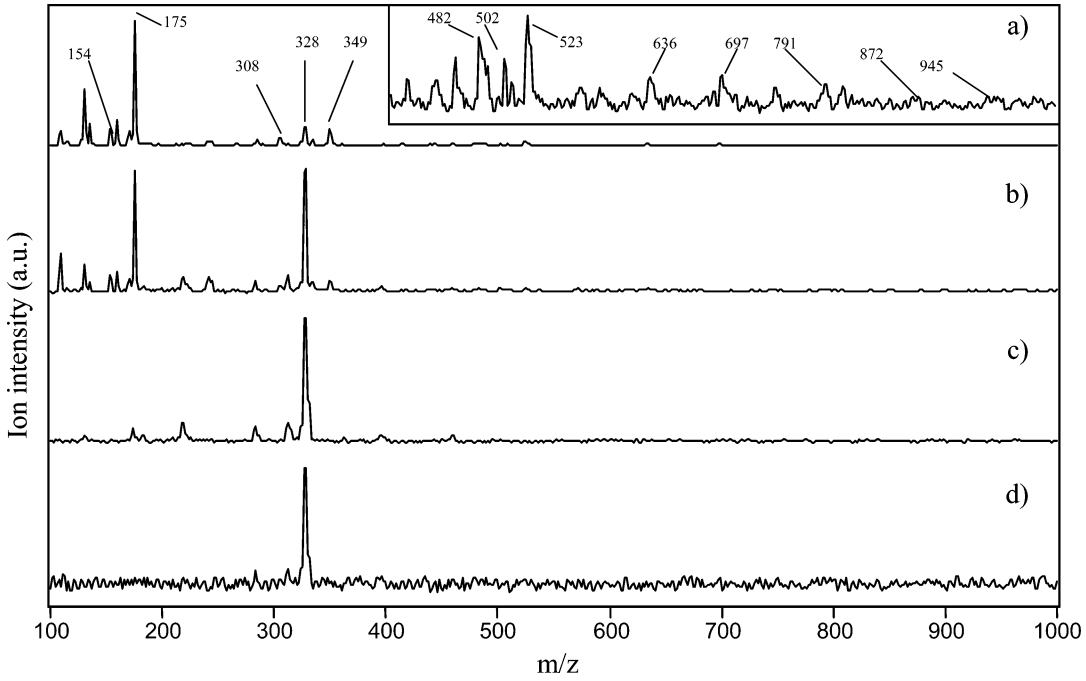

Figure 3. 308-nm laser ionization mass spectra of arginine−DHB clusters at ionization laser powers of (a) 95.7 MW/cm^2, (b) 32.7 MW/cm^2, (c) 3.96 MW/cm^2, and (d) 1.13 MW/cm^2.

TABLE 1: Structural Assignments and *m/z* Values of Various Species Observed in the Laser Ionization Mass Spectra of DHB/R Clusters

m/z	species
154	$DHB^{+\bullet}$
175	RH^+
308	$DHB_2^{+\bullet}$
328	$DHB_1R_1^{+\bullet}$
349	R_2H^+
482	$DHB_2R_1^{+\bullet}$
502	$DHB_1R_2^{+\bullet}$
523	R_3H^+
636	$DHB_3R_1^{+\bullet}$
697	R_4H^+
791	$DHB_4R_1^{+\bullet}$
872	R_5H^+
945	$DHB_5R_1^{+\bullet}$

translational dimensions (T_D). For example, $T_D = 1$ implies that all unit cells within one of the central cell are included, or a total of $3^3 = 27$ unit cells. For $T_D = 2$, there are $5^3 = 125$ unit cells, etc. To ensure convergence, the vertical IEs were calculated for clusters with T_D up to 5 at the HF/6-31+G** level.

Results and Discussion

Ionization Laser Power Studies at 308 and 266 nm. A series of mass spectra acquired using 308-nm radiation with increasing powers to ionize the DHB/R clusters are shown in Figure 3. At the lowest laser power used (1.13 MW/cm^2), a signal at *m/z* 328 is exclusively observed, which may be assigned to $DHB_1R_1^{+\bullet}$. As the ionization laser power is increased, a number of other ion signals are observable with the signal at *m/z* 175, corresponding to protonated arginine, RH^+, dominating the higher-power mass spectra. The remaining weaker-intensity ion signals observed in the higher-power mass spectra can be assigned to various homomolecular and heteromolecular clusters of DHB and R as well as fragments of these two species (see Table 1). The low relative intensities of the larger DHB_nR_m cluster ions contrasts with our previous studies of DHB/proline[15] and DHB/VPL[14] (VPL = valine-proline-leucine) clusters where significant ion-signal intensities are observed for larger clusters even at low ionization laser powers. This behavior suggests that the DHB_1R_1 cluster is particularly stable as compared with other larger DHB_nR_m combinations.

A 308-nm ionization laser power study, in which the log of the integrated $DHB_1R_1^{+\bullet}$ ion signal is plotted vs the log of the ionization laser intensity (log(I)), yields a slope of 1.97, suggesting that two 308 photons are needed to ionize the DHB_1R_1 cluster. This result is consistent with expectations given that the two-photon energy at 308 nm (8.05 eV) exceeds the IE of free DHB (8.0475 eV).[16] The distinctive increase in the intensity of RH^+ relative to $DHB_1R_1^{+\bullet}$ with increases in 308-nm laser power suggest that it requires one additional photon to dissociate the $DHB_1R_1^{+\bullet}$ cluster with the preferred dissociation pathway leading to RH^+ and $(DHB-H^+)^\bullet$. Indeed a plot of $\log(RH^+/DHB_1R_1^{+\bullet})$ vs log(I) yields a slope of 1.2, supporting the interpretation that a third 308-nm photon must be absorbed by the DHB_1R_1 clusters to both ionize and dissociate these species. These interpretations of the power-dependent behavior of the DHB/R clusters are consistent with our previous studies of DHB/proline[15] and DHB/VPL[14] clusters.

A sample mass spectrum acquired using 266-nm radiation at 11.2 MW/cm^2 to ionize the DHB/R clusters is shown in Figure 4. This laser power is near the threshold for ion formation at 266 nm, and a number of the signals observed may be assigned to background ionization of source region contaminant species at this shorter wavelength. These background species are indicated with an asterisk. Ion signals that may be associated with the DHB/R clusters are identified by their *m/z* in Figure 4 and assigned in Table 1. In contrast to the 308 nm mass spectra, even at this near-threshold ionization laser power, signals from both $DHB_1R_1^{+\bullet}$ and RH^+ are observed. Efforts to acquire 266-nm mass spectra at even lower ionization laser powers yielded no change in the relative $DHB_1R_1^{+\bullet}$ to RH^+ ion signals to the limit of their detection. This result indicates that absorption by the DHB_1R_1 cluster of two photons at 266 nm (9.32 eV) provides sufficient energy to both ionize and dissociate the cluster.

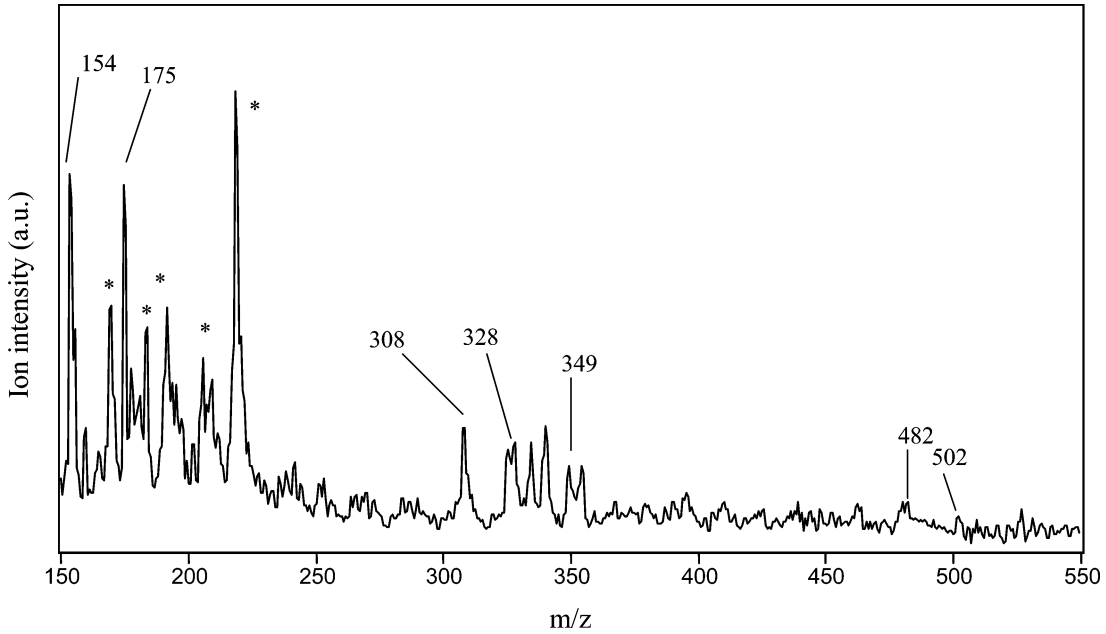

Figure 4. 266-nm laser ionization mass spectrum of arginine−DHB clusters at 11.2 MW/cm^2.

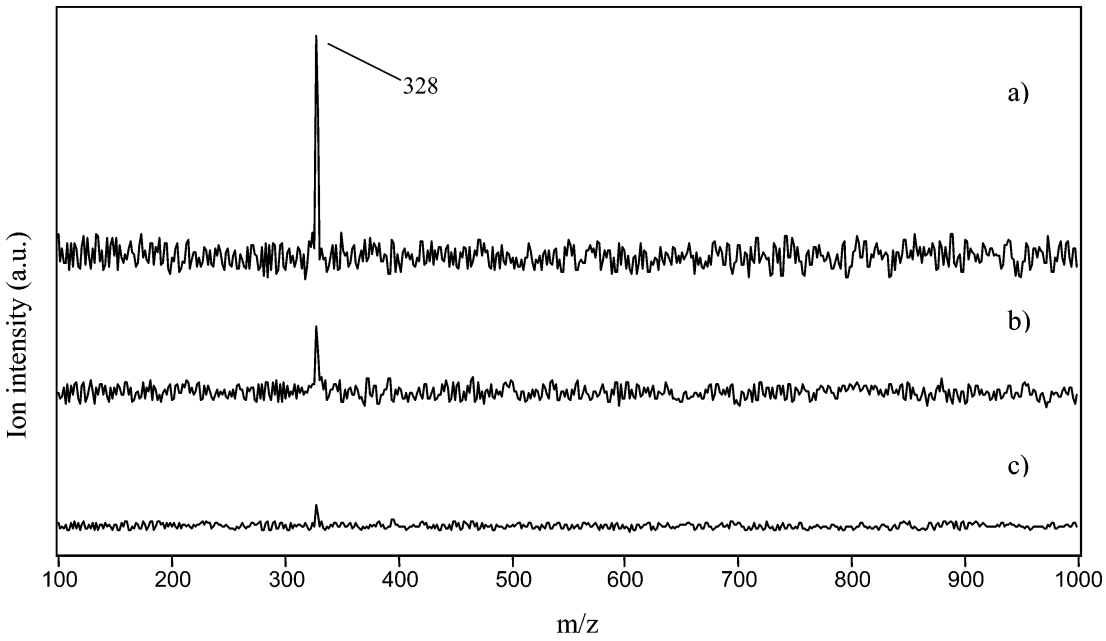

Figure 5. Laser ionization mass spectra of arginine−DHB clusters at (a) 338 nm, (b) 345 nm, and (c) 349 nm, respectively.

Cluster Ionization Energy Determination. From the power studies at 308 nm, an upper limit of 8.05 eV and a lower limit of 4.025 eV for the DHB_1R_1 cluster IE is established. To determine the actual IE of the DHB_1R_1 cluster, the ionization laser is sequentially scanned to wavelengths longer than 308 nm while monitoring the cluster ionization mass spectra. Examples of the threshold ionization mass spectra obtained at 338, 345, and 349 nm are shown in Figure 5. A photoionization efficiency (PIE) curve may be obtained by plotting the integrated intensity of the $DHB_1R_1^{+\bullet}$ ion signal vs the two-photon energy at the various wavelengths investigated. The region of the PIE curve where the sharp onset of the $DHB_1R_1^{+\bullet}$ is observed is shown in Figure 6.

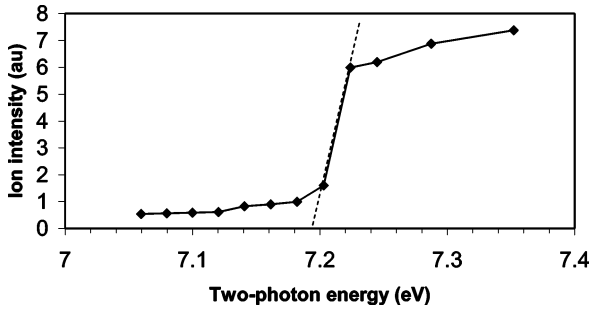

Figure 6. Photoionization efficiency curve obtained from one-color laser ionization mass spectra of arginine−DHB clusters taken at wavelengths between 338 and 352 nm.

Confirmation that the $DHB_1R_1^{+\bullet}$ ion signals recorded at these longer wavelengths result from two-photon processes is obtained in two ways. First, it is observed that no RH^+ ion is evident in the threshold ionization mass spectra. Appearance of RH^+ in the mass spectra would be expected if the ions result from three-photon processes since the three-photon energies at these wavelengths exceed the 9.32-eV two-photon energy at 266 nm,

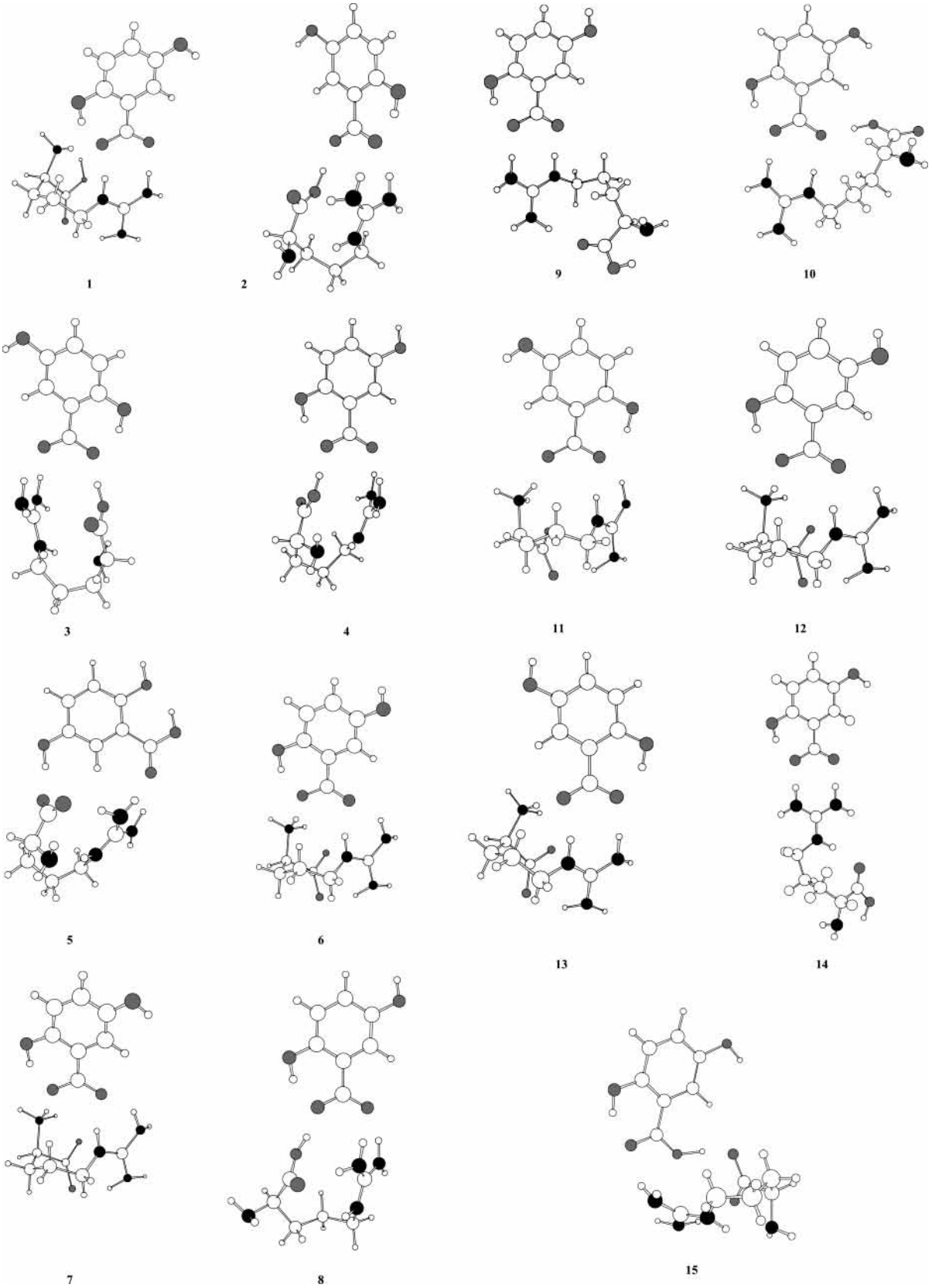

Figure 7. Fifteen minima for the arginine−DHB gas-phase complex at the B3LYP/6-31+G** level.

an energy already shown to lead to both ionization and dissociation of the clusters. Further support of two-photon ionization occurring at these longer wavelengths was obtained from a power study performed at 345 nm, near the onset threshold for ion formation, which yielded a slope of 2.06. With this confirmation of the two-photon ionization process, an extrapolation of the sharp onset observed in the PIE curve leads to an estimated IE for DHB_1R_1 of 7.193 eV.

Gas-Phase Modeling. Remarkably, there exist 15 distinct minima (Figure 7) within 5.3 kcal/mol of each other at the B3LYP/6-311++G(2df,2p)//B3LYP/6-31+G** level (Table 2). None of these structures are of type I (canonical arginine +

TABLE 2: Calculated Relative Energies and Ionization Energies of the Conformers[a,b,c]

	B3LYP/ 6-31+G**		B3LYP/ 6-311++G(2df,2p)		MP2/ 6-31+G(2df,2p)
conformer	relative energy	IP	relative energy	IP (in eV)	relative energy
1	0.00	7.21	0.00	7.22	0.00
2	0.34	7.12	0.73	7.12	0.61
3	0.29	7.12	0.83	7.13	0.42
4	0.92	7.11	1.33	7.11	1.04
5	1.20	7.09	1.36	7.10	1.47
6	2.73	6.88	2.02	6.89	7.51
7	2.67	7.35	2.99	7.36	2.14
8	3.43	7.15	3.04	7.17	5.46
9	3.82	6.92	3.33	6.93	9.04
10	4.58	7.21	3.35	7.22	6.61
11	3.03	7.34	3.38	7.35	2.65
12	3.13	7.33	3.41	7.34	2.59
13	3.36	7.41	3.65	7.42	2.35
14	4.98	6.79	4.03	6.80	10.59
15	5.02	7.55	5.25	7.55	4.54

[a] All energies were evaluated at the B3LYP/6-31+G** optimized geometries. [b] IE is in eV, ΔE in kcal/mol. [c] At the B3LYP/6-31+G** level, the relative free energies for structures 1−15 at 298.15 K are (in kcal/mol): 0.00, −0.18, 0.32, 0.68, −0.19, 6.70, 3.62, 1.93, 0.60, 1.91, 3.71, 3.90, 4.45, 1.15, and 4.45.

TABLE 3: Crystal Data and Summary of Data Collection and Refinement

formula	$C_{13}H_{20}N_4O_6 \cdot H_2O$
FW	346.35
cryst syst	monoclinic
space group	*P*2(1)
T, K	298
a, Å	5.3104(3)
b, Å	18.446(2)
c, Å	8.1639(6))
α, deg	90
β, deg	94.319(5)
γ, deg	90
V, Å^3	797.43(12)
Z	2
ρ(calc), g/cm^3	1.442
*R*1, w*R*2 ($I > 2\sigma(I)$)	0.0244, 0.0665
*R*1, w*R*2 (all data)	0.0255, 0.0674

DHB). In all but two of the clusters (5 and 15), the DHB is deprotonated and the arginine is protonated, forming an ion pair cluster. The first five conformers are also predicted to be the lowest-energy structures at the MP2/6-31+G(2df,2p)//B3LYP/6-31+G** level. Since the temperature of the clusters is not known experimentally, two different assumptions were made. At 50 K, we obtain a Boltzmann-averaged IE of 7.14 eV, while at 298.15 K, the corresponding value is 7.11 eV. Both values are in very good agreement with the experimental value of 7.193 eV.

X-ray Crystallography. The X-ray structure (Figure 2) shows that arginine and DHB crystallize as a 1:1 adduct. There is also a molecule of water in the asymmetric unit. All the hydrogens were located from the difference map and refined with isotropic displacement parameters. Crystal data are summarized in Table 3, while selected bond lengths and angles are presented in Table 4. Closer examination of the solid-state structure indicates that arginine exists in the zwitterionic form. In addition, one of the basic nitrogen sites of arginine accepts the proton from carboxylic acid moiety of the DHB leading to the formation of an ion pair. The N···H and O···H hydrogen bonds between water, arginine, and DHB lead to a network structure (see Figure 8). The water molecule serves as a bridge between one of the DHB molecules and two arginine units.

TABLE 4: Selected Bond Lengths (Å) and Angles (deg) Obtained from Crystal Structure Analysis

O(1)−C(7)	1.276(2)	C(1)−C(6)	1.387(3)
O(2)−C(7)	1.247(3)	C(1)−C(2)	1.398(3)
O(3)−C(2)	1.369(2)	C(1)−C(7)	1.506(2)
O(3)−H(3A)	0.92(3)	C(2)−C(3)	1.390(3)
O(4)−C(5)	1.374(3)	C(3)−C(4)	1.386(3)
O(5)−C(8)	1.249(2)	C(4)−C(5)	1.385(3)
O(6)−C(8)	1.251(2)	C(5)−C(6)	1.389(3)
N(1)−C(13)	1.318(3)	C(8)−C(9)	1.532(2)
N(2)−C(13)	1.329(3)	C(9)−C(10)	1.531(3)
N(3)−C(9)	1.487(2)	C(10)−C(11)	1.526(3)
N(4)−C(13)	1.325(3)	C(11)−C(12)	1.513(3)
N(4)−C(12)	1.452(3)		
C(13)−N(4)−C(12)	124.01(17)	O(1)−C(7)−C(1)	117.01(17)
C(6)−C(1)−C(2)	119.59(17)	C(1)−C(6)−C(5)	120.70(19)
C(6)−C(1)−C(7)	119.95(17)	O(5)−C(8)−O(6)	126.98(17)
C(2)−C(1)−C(7)	120.43(17)	O(5)−C(8)−C(9)	115.97(16)
O(3)−C(2)−C(3)	118.78(18)	O(6)−C(8)−C(9)	116.99(18)
O(3)−C(2)−C(1)	121.77(17)	N(3)−C(9)−C(10)	110.54(16)
C(3)−C(2)−C(1)	119.44(18)	N(3)−C(9)−C(8)	109.39(15)
C(4)−C(3)−C(2)	120.5(2)	C(10)−C(9)−C(8)	111.32(15)
C(5)−C(4)−C(3)	120.12(19)	C(11)−C(10)−C(9)	114.79(15)
O(4)−C(5)−C(4)	117.96(17)	C(12)−C(11)−C(10)	110.95(15)
O(4)−C(5)−C(6)	122.4(2)	N(4)−C(12)−C(11)	108.90(16)
C(4)−C(5)−C(6)	119.6(2)	N(1)-C(13)−N(4)	119.41(18)
O(2)−C(7)−O(1)	123.47(17)	N(1)−C(13)−N(2)	119.7(2)
O(2)−C(7)−C(1)	119.51(17)		
N(4)−C(13)−N(2)	120.92(18)		

Many studies of the structure of arginine and the importance of the guanidinium group have appeared in the literature.[28−30] It is known that the most important hydrogen bonds are the ones involving the guanidinium group. Because of the presence of the positive charge, the guanidinium group interacts strongly with negatively charged groups such as carboxylate. Salunke and Vijayan have observed the specific interactions of the guanidinium group in different crystal structures.[31] They observed four different types of specific interactions of the guanidinium group with carboxylate or phosphate groups, depending upon which two NH groups are involved in hydrogen bonding and whether there are one or two oxygen-atom acceptors. The most common situation is that two NH groups are hydrogen bonded to two distinct oxygen atoms, and that is exactly what is seen here in several of the gas-phase minima. Indeed, both the cocrystal and the low-energy gas phase 1:1 adduct show identical hydrogen bonding arrangements between the guanidinium group and the carboxylic acid group (type B in the scheme of Salunke and Vijayan).

Solid-State Modeling. To investigate the effects of the crystal environment on the electronic structure, electron-detachment energy of free anionic DHB and IEs of several clusters simulating the (arg)DHB cocrystal (see calculations section) have been calculated at the HF/6-31+G** level and are reported in Table 5. The calculated IE increases from 3.09 eV for the free DHB anion to 6.47 eV for the fundamental structural unit (Figure 2). The IE further increases to 8.51 eV for the largest cluster, although it does not appreciably change beyond $T_D = 1$ (see calculations section for the definition of T_D). To check on the accuracy of the calculated IE at the HF level, we recalculated it at the B3LYP/6-31+G** level for the $T_D = 5$ cluster and found a value of 8.33 eV, in excellent agreement with the HF value of 8.51 eV. A similar increase in IE with cluster size was found for the KTIE. The significant increase in the KTIE on going from the free DHB anion (4.53 eV) to the fundamental structural unit (7.18 eV) and then to the largest cocrystal (8.78 eV) clearly shows that the IE increase is primarily due to a ground-state effect. This effect is easy to understand. Short-term hydrogen bonding, as modeled in the

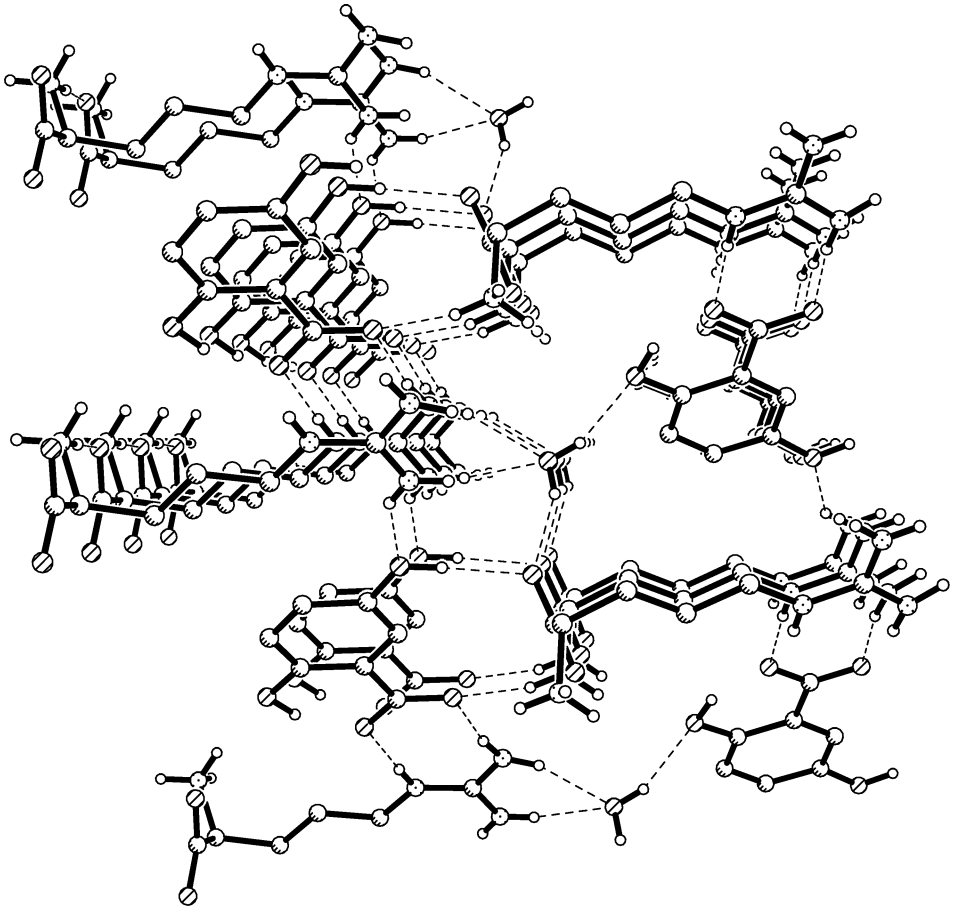

Figure 8. Small portion of the cocrystal structure showing close contacts (all the hydrogen atoms on carbons have been removed for clarity).

TABLE 5: Calculated Vertical IEs and KTIEs of the Free DHB Anion, the Fundamental Structural Unit, and Large Cocrystals with Different Sizes at the HF/6-31+G Level[a]**

cluster	IE (eV)	KTIE (eV)	T_D
[DHB][b]	3.09[c]	4.53	0
[DHB·Arg·H_2O][d]	6.47	7.18	0
[DHB·Arg·H_2O]$DHB_{53}Arg_{53}(H_2O)_{53}$	8.33	7.25	1
[DHB·Arg·H_2O]$DHB_{249}Arg_{249}(H_2O)_{249}$	8.47	8.43	2
[DHB·Arg·H_2O)]$DHB_{685}Arg_{685}(H_2O)_{685}$	8.49	8.68	3
[DHB·Arg·H_2O]$DHB_{1457}Arg_{1457}(H_2O)_{1457}$	8.50	8.75	4
[DHB·Arg·H_2O)]$DHB_{2661}Arg_{2661}(H_2O)_{2661}$	8.51	8.78	5

[a] The species in the square brackets are treated explicitly at the HF level. The species outside the square brackets are treated by point charges. See text for the definition of T_D. [b] Deprotonated. [c] Electron-detachment energy. [d] See Figure 2.

fundamental structural unit, clearly stabilized the DHB anion. Similarily, long-range Coulombic effects, as modeled by the point charges, must also be important in stabilizing this fundamentally ionic cocrystal. What *is* surprising, however, is that the IE of DHB in the cocrystal, although technically an anion, is actually slightly *higher* that that of free neutral DHB (8.05 eV from experiment, 8.11 eV calculated at the B3LYP/6.31G** level).

Conclusions

There is a remarkable similarity between the lowest-energy structures of the 1:1 adduct of arginine and DHB in the gas phase and the solid-state cocrystal. In both cases, the dominant intermolecular interaction is a double hydrogen bond between the guanidinium group of arginine and the (deprotonated) carboxylate group of DHB. While the energies of these conformers are far too close to definitively conclude which is the ground-state structure, it is remarkable that thirteen of the fifteen conformers are ion pairs in the gas phase.

Acknowledgment. D.S.M. thanks the Welch Foundation (Grant Y-0743), H.R.V.D. thanks the Welch Foundation (Grant Y-1289), and G.K. thanks the Welch Foundation (Grant Y-1463) for support of this work.

Supporting Information Available: Optimized Cartesian coordinates for conformers 1−15 and X-ray crystallographic files in the CIF format for the arginine−DHB cocrystal are available free of charge via the Internet at http://pubs.acs.org.

References and Notes

(1) (a) Locke, M. J.; Hunter, R. L.; McIver, R. T. *J. Am. Chem. Soc.* **1979**, *101*, 272. (b) Locke, M. J.; McIver, R. T. *J. Am. Chem. Soc.* **1983**, *105*, 4226.

(2) (a) Jenson, J. H.; Gordon, M. S. *J. Am. Chem. Soc.* **1995**, *117*, 8159−8170. (b) Bertran, J.; Rodriguez-Santiago, L.; Sodupe, M. *J. Phys. Chem. B.* **1999**, *103*, 2310.

(3) Ding, Y.; Kroug-Jesperson, K. *Chem. Phys. Lett.* **1992**, *199*, 261

(4) Price, W. D.; Jockusch, R. A.; Williams, E. R. *J. Am. Chem. Soc.* **1997**, *119*, 11988.

(5) Chapo, C. J.; Paul, J. B.; Roth, K.; Saykally, R. J. *J. Am. Chem. Soc.* **1998**, *120*, 12956.

(6) (a) Maksic, Z. B.; Kovacevic, B. *J. Chem. Soc., Perkin Trans. 2* **1999**, 2623. (b) Skurski, P.; Gutowski, M.; Barrios, R.; Simons. J. *Chem. Phys. Lett.* **2001**, *337*, 143.

(7) Price, W. D.; Jockusch, R. A.; Williams, E. R. *J. Am. Chem. Soc.* **1997**, *119*, 11988.

(8) Chapo, C. J.; Paul, J. B.; Roth, K.; Saykally, R. J. *J. Am. Chem. Soc.* **1998**, *120*, 12956.

(9) Rak, J.; Skurski, P.; Simons, J.; Gutowski, M. *J. Am. Chem. Soc.* **2001**, *123*, 11695.

(10) Julian, R. R.; Beauchamp, J. L.; Goddard, W. A. *J. Phys. Chem.* **2002**, *106*, 32.
(11) Zenobi, R.; Knochenmuss, R. *Mass Spectrom. Rev.* **1999**, *17*, 337.
(12) Land, C. M.; Kinsel, G. R. *J. Am. Soc. Mass Spectrom.* **1998**, *9*, 1060.
(13) Land, C. M.; Kinsel, G. R. *Eur. Mass Spectrom.* **1999**, *5*, 117.
(14) Land, C. M.; Kinsel, G. R. *J. Am. Soc. Mass Spectrom.* **2001**, *12*, 726.
(15) Kinsel, G. R.; Knochenmuss, R.; Setz, P.; Land, C. M.; Goh, S.-K.; Archibong, E. F.; Hardesty, J. H.; Marynick, D. S. *J. Mass Spectrom.* **2002**, *37*, 1131.
(16) Karbach, V.; Knochenmuss, R. *Rapid Commun. Mass Spectrom.* **1998**, *12*, 968.
(17) Allinger, N. L. *J. Am. Chem. Soc.* **1977**, *99*, 8127.
(18) Cornell, W. D.; Cieplak, P.; Bayly, C. I.; Gould, I. R.; Merz, K. M.; Ferguson, D. M.; Spellmeyer, D. C.; Fox, T.; Caldwell, J. W.; Kollman, P. A. *J. Am. Chem. Soc.* **1995**, *117*, 5179.
(19) Halgren, T. A. *J. Comput. Chem.* **1996**, *17*, 490.
(20) (a) Becke, A. D. *J. Chem. Phys.* **1993**, *98*, 5648. (b) Lee, C.; Yang, W.; Parr, R. G. *Phys. Rev. B* **1988**, *37*, 785.
(21) Ditchfield, R.; Henre, W. J.; Pople, J. A. *J. Chem. Phys.* **1971**, *54*, 724.
(22) Krishnan, R.; Binkley, J. S.; Seeger, R.; Pople, J. A. *J. Chem. Phys.* **1980**, *72*, 650.
(23) IEs were not calculated at the MP2 level because of the high degree of spin contamination in the Hartree−Fock wave functions of the ion states ($S^2 \approx 0.96$).
(24) Mohamadi, F.; Richards, N. G. J.; Guida, W. C.; Liskamp, R.; Lipton, M.; Caufield, C.; Chang, G.; Hendrickson, T.; Still, W. C. *J. Comput. Chem.* **1990**, *11*, 440.
(25) Frisch, M. J.; Trucks, G. W.; Schlegel, H. B.; Scuseria, G. E.; Robb, M. A.; Cheeseman, J. R.; Zakrzewski, V. G.; Montgomery, J. A., Jr.; Stratmann, R. E.; Burant, J. C.; Dapprich, S.; Millam, J. M.; Daniels, A. D.; Kudin, K. N.; Strain, M. C.; Farkas, O.; Tomasi, J.; Barone, V.; Cossi, M.; Cammi, R.; Mennucci, B.; Pomelli, C.; Adamo, C.; Clifford, S.; Ochterski, J.; Petersson, G. A.; Ayala, P. Y.; Cui, Q.; Morokuma, K.; Malick, D. K.; Rabuck, A. D.; Raghavachari, K.; Foresman, J. B.; Cioslowski, J.; Ortiz, J. V.; Stefanov, B. B.; Liu, G.; Liashenko, A.; Piskorz, P.; Komaromi, I.; Gomperts, R.; Martin, R. L.; Fox, D. J.; Keith, T.; Al-Laham, M. A.; Peng, C. Y.; Nanayakkara, A.; Gonzalez, C.; Challacombe, M.; Gill, P. M. W.; Johnson, B. G.; Chen, W.; Wong, M. W.; Andres, J. L.; Head-Gordon, M.; Replogle, E. S.; Pople, J. A. *Gaussian 98*, revision A.9; Gaussian, Inc.: Pittsburgh, PA, 1998.
(26) *Handbook of Chemistry and Physics, 60th ed.*; CRC Press, Inc.: Boca Raton, Fl, 1979−80.
(27) Koopmans, T. *Physica* **1933**, *1*, 104.
(28) Karle, I. L.; Karle, J. *Acta Crystallogr.* **1964**, *17*, 835.
(29) Lehmann, M. S.; Verbist, J. J.; Hamilton, W. C.; Koetzle, T. F. *J. Chem. Soc.* **1973**, *2*, 133.
(30) Silva, M. R.; Paixão, J. A.; Beja, A. M.; Da Veiga, L. A. *J Chem. Cryst.* **2000**, *30*, 411.
(31) Salunke, D. M.; Vijayan, M. *Int. J. Peptide Protein Res.* **1981**, *18*, 348.